Evaluation of turbulence-related high-frequency tidal current velocity fluctuation

P. Garcia Novo, Y. Kyozuka, M.J. Ginzo-Villamayor

Version: Accepted Manuscript

HOW TO CITE

García Novo, P., Kyozuka, Y., Ginzo-Villamayor, M.J. (2019). Evaluation of turbulence-related high-frequency tidal current velocity fluctuation Renewable Energy. 139. pp. 313-325.

FUNDING

The authors would like to thank the Ministry of Environment of Japan for permission to publish of the data used in this study, which were obtained through the project for Promotion of Realization of Tidal Current Power Generation supported by the ministry in 2014 and 2015.

Abstract

Within the development needed for economy viability of tidal stream energy, adaptability of laboratory converters to sea flow conditions is a milestone. The objective of this work is to investigate the high frequency fluctuations in currennt velocity magnitude and direction related to the turbulent nature of the flow and present a new method for their prediction. With this purpose, high frequency data measured by two ADV (32 Hz) and two ADCP (8 Hz) at four different points in the sea area surrounding Goto Islands (Japan) are analyzed. The data were divided in short-time samples (3-minutes data for ADV and 5-minutes data for ADCP) and treated separately. Velocity magnitude fits a normal distribution, with prediction levels higher than 95% for a margin of error of 0.25 m/s when comparing different percentiles between 0.1 and 99.9. Flow direction is analyzed in terms of opening angle between two representative percentiles equidistant from the median(99.9-0.1, 95-5,...), giving as a result a leptokurtic distribution, more outlier-prone than normal. Empirically, for opening angles 99.9-0.1, 97.7-2.3 and 95-5, slopes of 6.79 (6 in normal distribution), 4.17 (4) and 3.38 (3.29) were found, with results similar to a theoretical normal distribution for narrower angles. The new prediction method for high frequency fluctuations is based in this direct correlation between velocity magnitude and direction fluctuations with turbulence intensity and transverse turbulence intensity, respectively. These two parameters can be estimated indirectly by numerical models, giving rise to a tool for the prediction of turbulence-related high frequency fluctuation.

Keywords— Tidal energy, Turbulence, ADCP, ADV

Evaluation of turbulence-related high-frequency tidal current velocity fluctuation

Patxi Garcia Novo, Yusaku Kyozuka, Maria Jose Ginzo Villamayor

January 21, 2019

1 Introduction

Tidal stream energy has been presented as one of the most promising renewable energy options among other reasons due to the high prediction level of available resource. Tides can be defined as the sum of constituent components as a result of the interaction between Earth, Sun and Moon gravitational attractions, expressed mathematically as [1]:

$$\zeta = \sum_{i=0}^{n} a_i \cos(\omega_i t + \varphi_i) \tag{1}$$

being t the time; a_i the angular frequency dependent on the relative movement between Earth, Sun and Moon; and ω_i and φ_i the amplitude and phase, respectively, for each tide constituent, which varies according to the geographical position. This definition has been a base for widely proven tide level prediction methods [2, 3].

Harmonic forcing simulating tide conditions has been also used for numerical modelling-based tidal stream energy assessment works [4, 5, 6], with good agreement both in terms of water level [4] and tidal velocity [5, 6] when comparing 3-minutes averaged [6] measured data with prediction results.

Nevertheless, when thinking on energy extraction, not only tides but also currents must be taken into account. In this regard, despite the capability of harmonic analysis based approaches to predict averaged tidal current velocities [5, 6], there are certain current properties (three-dimensional nature, effect of local geomorphology and non-sinusoidal characteristics such as sub-tidal variations, supra-tidal variations or turbulence) differentiable from tides which limit these methods for current evaluation. This issue was already pointed a few decades ago by Godin [7], who concluded that currents cannot be predicted with the same level of precision as the tide. These variations from the harmonic analysis-based estimation have meaningful consequences in the turbine loads [8], making of this a key point for tidal stream energy technologies. A case that clearly exemplifies this statement is the failure of an OpenHydro turbine in the Bay of Fundy in November 2009, due to tidal flows that were two and a half times stronger than expected [9].

With the aim of getting a better understanding of tidal currents, Polagye et al [10] analyzed high frequency velocity data measured in Puget Sound, observing two kinds of variations. First, non-sinusoidal fluctuations over time scales around 1 hour, which, although cannot be estimated by harmonic analysis, exhibit a certain degree of periodicity, allowing its description by site-specific empirical functions which must include ebb and flood variations or diurnal inequality. Second, turbulence related fluctuation over time scales under one minute. This fluctuation was found more important than the first one in terms of magnitude (over 0.5 m/s for peak currents) and it was considered unpredictable.

Regarding this second fluctuation type, although its effect on energy potential estimation is lower, its study is necessary for turbine design considerations, such us blade loads, support structures, seabed connections [11] or devices stabilization on the bottom by the generation of down force from the tidal flow [12]. For these reasons, several authors have carried out turbulence studies at potential tidal stream energy exploitation sites based on velocity measurement. In these studies, besides the calculation of representative turbulent related parameters such as turbulence intensity, turbulent kinetic energy or integral time and length scales, whose characterization is also crucial for turbine design due to its effect on blade loads, power and thrust coefficients or wake characteristics [13, 14, 15, 16], high frequency velocity fluctuation was also analyzed. In this respect, velocity fluctuations within a range higher than 1 m/s during a 1-minute period for which averaged value was approximately 2 m/s were found in the streamwise signal of an ADV measurements in the Sound of Islay [17]. Also, in Kobe Strait [18], instantaneous streamwise velocities between 0.5 m/s and 2.5 m/s were observed with an ADCP for a 5-minute averaged value of 1.5 m/s.

Recently, the efforts of tidal energy researchers have been focused on the prediction of turbulence conditions at a given location. On this point, results from turbulence models simulating current conditions at tidal stream energy sites able to estimate turbulent kinetic energy have been recently published [19]. In terms of velocity fluctuation, Harding et al [11] presented a long-term prediction method for extreme velocities (higher and lower than the averaged) based on 32 Hz and 2 Hz velocity data measured by an ADV and an ADCP, respectively, simultaneously and at the same point in Puget Sound. With one month data, a 50-year velocity perturbation from a 64s mean velocity could be predicted. However, the results show considerable discrepancies between the measurements of both devices and "several years of data is required to perform the analysis to an acceptable level of confidence".

In this context, this study attempts to seek a new method to predict turbulence related velocity perturbations both in terms of magnitude and direction, thus reducing the need for in-situ measurement, following the Godin [7] suggestion that "the study of currents is essentially a research problem and should not be considered a matter for routine data processing at the clerical or technical level". The present proposal is based on the analysis of data measured by two 32 Hz ADVs (Acoustic Doppler Velocimeter) and two 8 Hz ADCPs (Acoustic Doppler Current Profiler) at four different points in Goto Islands, Japan.

2 Materials and Methods

2.1 Location

Located in Nagasaki Prefecture, southwestern Japan, between the Strait of Korea and the Pacific Ocean, Goto Islands is an archipelago formed by 140 islands (see Fig.1). Five of these islands form four main channels (from west to east, Tanoura Strait, Naru Strait, Takigawara Strait, and Wakamatsu Strait). The big amount of water passing through these channels generates strong currents, making of this area a good location for tidal stream energy exploitation. Therefore, two of these channels (Tanoura Strait and Naru Strait) have been designated as a tidal energy test site by the Japanese government [20]. At this area, the tide type is typically mixed mainly semidiurnal, being M2 the main tidal constituent.

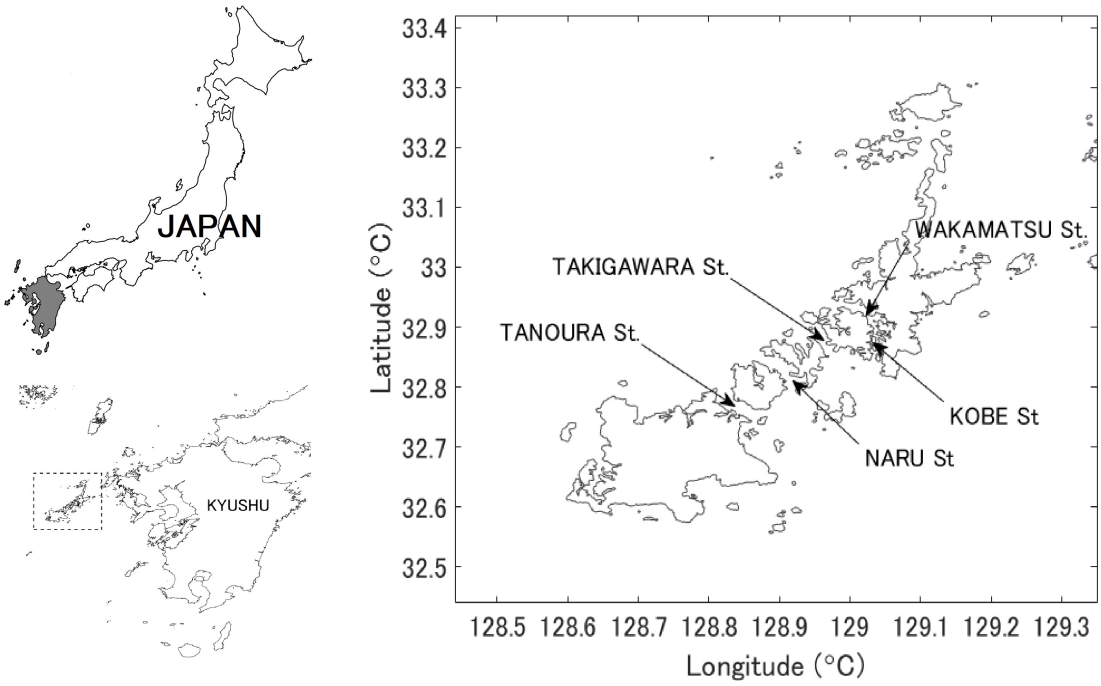

Figure 1: Tanoura Strait, Naru Strait and Kobe Strait in Goto Islands, Nagasaki Prefecture, Japan

The areas selected for measuring devices installation are Naru Strait, Tanoura Strait and Kobe Strait, a small semi-enclosed channel formed by an inner island in Wakamatsu Strait (for a more detailed description of these channels refer to [18, 21]). The importance of the first two channels lies in their high tidal stream energy potential, as mentioned in the previous paragraph. Kobe Strait, due to its lower depth and current velocity, could be a considerable option for testing low-velocity converter devices or in an earlier development stage. A brief description of the four measuring locations for this study is

presented below.

2.2 Data measurement

One Nortek Vector ADV was operating during 8 days from November 17th at 0:00h to November 24th at 17:10h in 2014 in (32°46'45.2"N, 128°50'3.1"E; hereafter P1), Tanoura Strait, between Fukue Island and Hisaka Island. The dimensions of this channel are 6 km length and 2 km width, approximately. Water flows in a SE-NW direction during flood tide and vice versa during ebb tide, with minor variations due to very local geomorphologic characteristics. In the southern mouth, water move is affected by Tatarajima Island, dividing the flow into two bifurcations. The sea bottom is mainly rocky. Focusing on the measuring point, it is located at nearly 200 m from Hisaka Island western coastline, where the averaged depth during the data collection period was 26.1 m. The ADV installed at 3 meter from the sea bottom at this point was set to measure during the first 3 minutes of every 10-minute period, followed by 7 minutes in stand-by. This device collects high resolution velocity, temperature and pressure data. The internal sampling rate is 250 Hz, while the sampling output rate was set as 32 Hz, thus collecting 5760 data for every 3-minute measuring period. The sampling volume dimensions are 15 mm diameter and 5 mm height. Its velocity measurement accuracy is 0.5% of the measured value ± 1 mm/s.

Simultaneously, in Naru Strait (32°49'41.1"N, 128°58'56.4"E; hereafter P2) a second Nortek Vector ADV, with the same characteristics above presented, was operating under analogous setup conditions. Naru channel length and width are approximately 7 km and 2 km, respectively, with the exceptions of the narrowing due to Kagaribisaki cape and Suetsujima Island. As with Tanoura Strait, bottom is mainly rocky and the main axis orientation is NW-SE. The averaged depth during the 8-days period at the ADV measuring point, nearly 300 m east of Warabikojima Island, was 24.6 m. At this same channel, at approximately 200 m east from the ADV measuring point (32°49'38.8"N, 128°54'3.7"E; hereafter P3), one Nortek Signature 1000 AD2CP was operational from April 14th until May 24th, 2016. Nevertheless, it must be said that quality of data collected during the last 15 days is not good enough to guarantee reliable results, so they were removed for further analysis. This device beam frequency and width are 1 MHz and 2.9°, respectively. The measuring sampling volume for each beam and layer is defined by a polyhedron of 142 mm height and 212 mm length, its minimum accuracy is a 0.3% of the measured value and the velocity resolution is 0.1 cm/s. This AD2CP was set to cyclically measure with an 8Hz sampling output rate during 5 minutes followed by 15 minutes in standby. The number of vertical layers is 22, 1 m width each one, with a blanking distance of 1 m. Since the time averaged depth during the measuring period was 35.0 m, approximately two-thirds of the water column were covered.

The same AD2CP had been operational from February 27th to March 14th, 2014, at (32°52'40.81"N, 129°01'46.79"E; hereafter P4) in Kobe Strait. At this point, where the time averaged depth during this 15-day period was 18.0 m, 36 vertical layers (0.5 m thickness) were measured with the same timing and frequency measuring setup (8 Hz, 5-minute on, 15-minute off) as previously presented for P3. The blanking distance was

set as 0.1 m. Due to the water column width limitations, data measured for the seven last vertical layers counting from the bottom (29 to 36) are unreal and not considered for the water flow analysis. Likewise, due to bottom interaction, an accurate measurement cannot be guaranteed in the deepest layer, so it is discarded.

2.3 Data treatment

2.3.1 Signal pretreatment

Previous to the velocity fluctuation and turbulence analysis, a data quality pretreatment is necessary. In the four cases, this pretreatment consisted of two steps: denoising and despiking. Noise was eliminated following the manufacturer recommendations, replacing points for which correlation is under 70% for the ADV signals [22] and under 50% for the AD2CP signals [23] by the linearly interpolated values. The already denoised signal was treated with a Kernel Density based algorithm developed by Islam and Zhu [24] and tested in this kind of data despiking. After noise elimination, 5-minute (ADCP) and 3-minute (ADV) averaged values for the three signals, one for each component of velocity, were calculated. Based on these averaged values and using a least square method which guarantees that the mean value of all the 5-minute or 3-minute averaged transverse velocities during the measuring period is null, a rotation angle is calculated to convert the original data to a streamwise (parallel to N-S axis), transverse (perpendicular to N-S axis) and vertical coordinate system. Rotation angles were calculated separately for flood and ebb tide and for each measuring point and vertical layer (in the case of ADCP). This data rotation allows a clearer analysis of the flow characteristics.

2.3.2 Velocity magnitude fluctuation

In order to analyze only turbulence-related variations and minimize the influence of other fluctuation generator factors, every data block corresponding to a 3-minute measuring period for ADV data and 5-minute measuring period for ADCP data was treated separately. The velocity magnitude fluctuations are parameterized by percentiles. For each data block, percentiles for each multiple of five from 5 to 95, as well as those percentiles corresponding with sigma integer multiplying factors for a theoretical normal distribution (0.1, 2.3, 15.9, 84.1, 97.7, 99.9), are extracted.

2.3.3 Current direction fluctuation

The analysis in the current direction fluctuation is analogous to the presented for velocity magnitude. Considering 0° for East and 90° for North, a numerical value is given for the direction observed for each 8 Hz (ADCP) or 32 Hz (ADV) measurement. With these values, the same percentiles presented in 2.1.2 are extracted from each 5-minute or 3-minute data block. Finally, assuming symmetry in short time period data, the fluctuation in the current direction is parameterized by opening angles between two percentiles equidistant from the median value (99.9-0.1, 97.7-2.3, 95-5,...). In this case, most of the 5-minute or 3-minute data blocks are "contaminated" with the current directions

collected from very low velocity magnitude points, resulting on opening angles much wider than those to be considered for tidal turbine designing purposes. In order to avoid this kind of contamination in the samples, instantaneous flow directions corresponding with velocity magnitudes lower than 0.5 m/s are excluded for the current direction analysis. A graphic summary of the procedure for the extraction of opening angles is presented in Fig 2, showing the opening angles between percentiles 99.9 and 0.1 and between percentiles 70 and 30.

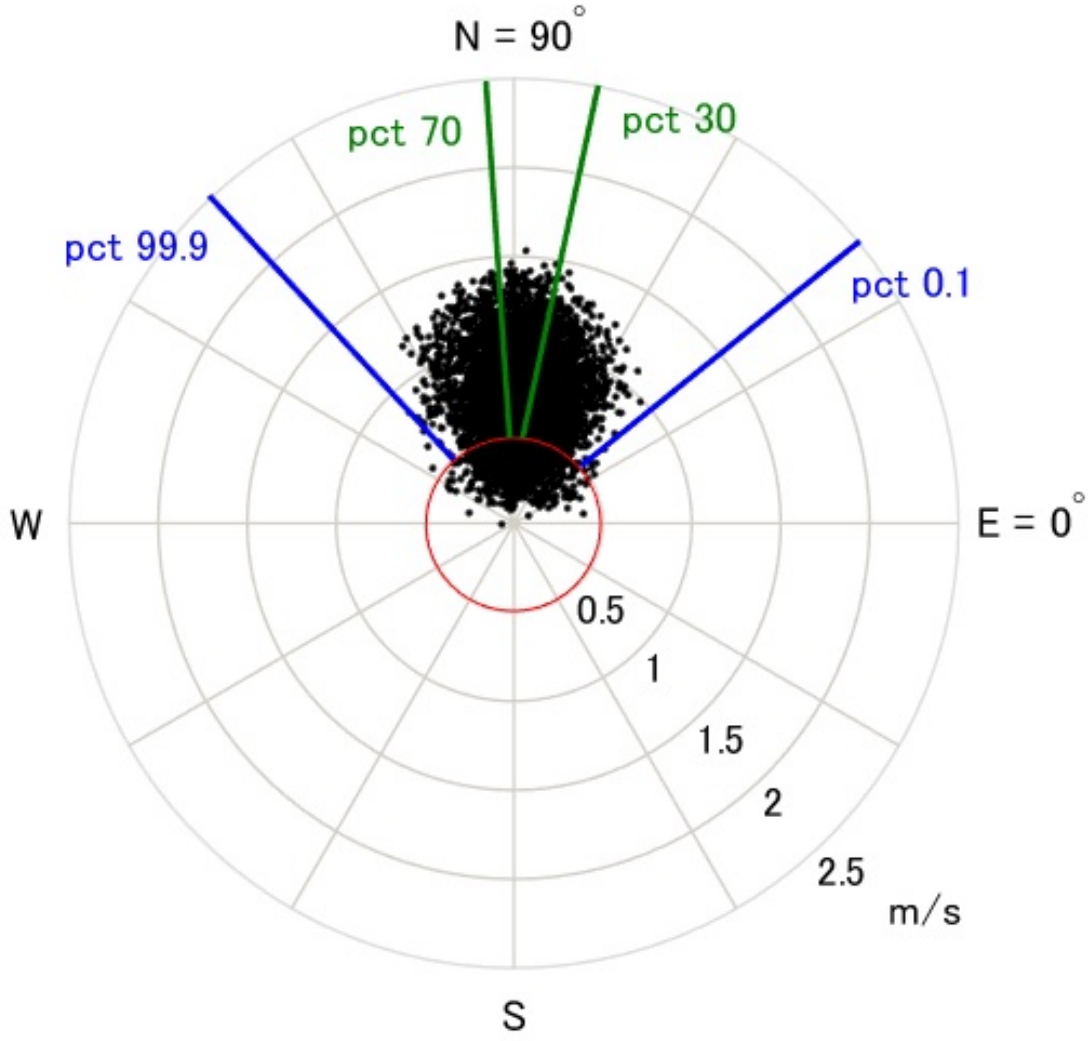

Figure 2: Graphic representation of opening angles extraction with pct 99.9 - pct 0.1 opening angle (blue), pct 70 - pct 30 opening angle (green) and 0.5 m/s threshold (red)

2.3.4 Turbulence intensity and prediction of velocity magnitude fluctuation

Laboratory tests have demonstrated the influence of turbulence intensity (TI) conditions to the converter devices in terms of fatigue [13]. Furthermore, higher turbulence intensity values lead to a reduction in the velocity deficit downstream, with the maximum deficit point closer to the converter [14]; and a small reduction in the averaged flapwise and edgewise blade root bending moments, though fluctuations increase [15]. For this reason, turbulence intensity is a key parameter for tidal stream energy converters design.

Turbulence intensity is defined for a given period of time as the ratio of standard deviation to averaged velocity magnitude (see Eq 2). Thus, when current velocity approaches zero, very high and unrepresentative values are obtained for turbulence intensity. This effect was observed and analyzed in previous similar studies, neglecting turbulence intensity results for defined "slack conditions" range for which tidal energy extraction is expected to be null [25]. In the present study, the upper limit for this range can be set at 0.7 m/s, a typical cut-in speed for tidal stream energy turbines [26], discarding all the 3-minute or 5-minute data blocks for which mean velocity is lower.

$$TI = \frac{\sigma_V}{\bar{V}} \tag{2}$$

Besides its effect on the converter behavior, summarized in the first paragraph in Section 2.3.4, in the present study turbulence intensity is used as a means for the prediction of the different percentiles of velocity magnitude. The election of turbulence intensity as the parameter used for this purpose is based on two reasons. First, the dimensionless nature of turbulence intensity, which makes the direct comparison with velocities possible. Second, the capability of numerical methods for its prediction. Turbulence intensity can be estimated from numerical model results for turbulent kinetic energy by $tke = \frac{3}{2}\left(U_{avg} \cdot TI\right)^2$ [19]. For a short period of time, in this case 5 (ADCP) or 3 (ADV) minutes, the direct correlation between a certain percentile α of velocity magnitude and turbulence intensity proposed in the present study is defined by Eq 3:

$$V_{p_\alpha} = \left(MF_M \cdot TI + 1\right) \cdot \bar{V} \tag{3}$$

Where V_{p_α} is the velocity magnitude value for a certain percentile, MF_M is a multiplier factor for that velocity magnitude percentile, and TI and $\bar{V}$ are the turbulence intensity and averaged velocity magnitude, respectively, for a 3-minute or 5-minute period. Physically, in a flow with no turbulence, velocity fluctuation is null. This is represented in the equation with the "+1" term.

The method to establish the MF_M for each percentile starts assuming and evaluating a theoretical normal distribution. If this does not fit the measured data, alternative values are calculated empirically. The procedure is as follows. From a first lineal approach, for which all the 3-minute (ADV) or 5-minute (ADCP) samples with mean velocity higher than 0.7 m/s are used, the 1% farthest poins are discarded in order to avoid outliers, calculating the final equations with the lineal regression of the remaining 99% points. The resulting 52 approaches (P1, P2, 22 layers in P3 and 28 layers in P4) are evaluated individually comparing them with the measured data at its corresponding

point and layer, obtaining the 15% prediction level for each case. With these results, a prorated averaged value for MF_M based on the individual slopes and their corresponding prediction levels is calculated.

2.3.5 Transverse turbulence intensity and prediction of current direction fluctuation

After the data rotation to the N-S parallel axis, current direction is mainly defined by the transverse component of velocity. For this reason, the prediction of the opening angles presented in Section 2.3.3 is based on the transverse turbulence intensity (TTI), defined as the ratio of the standard deviation of the transverse component of velocity by the averaged velocity magnitude (Eq 4):

$$TTI = \frac{\sigma_{v_t}}{\bar{V}} \tag{4}$$

As for TI, transverse turbulence intensity is dimensionless and can be estimated from numerical methods results for turbulent kinetic energy and assuming a theoretical relation between standard deviations of the streamwise, transverse and vertical components of velocity of σ_s:σ_t:σ_v=1:0.71:0.55, proposed by Nezu and Nakagawa [27] based on an experimental study with two-dimensional channel flows at relatively low Reynolds numbers. Similar ratios have been also observed by Milne et al [17] at a tidal stream power site (1:0.75:0.56).

Similarly to velocity magnitude, the proposed direct correlation between opening angles and transverse turbulence intensity for a short period of time is defined by Eq 5.

$$OA_{q_\alpha, q_{1-\alpha}} = (2 \cdot MF_D \cdot TTI) \tag{5}$$

Where OA is the opening angle for a given pair of percentiles $(q_\alpha, q_{1-\alpha})$ for a 3-minute or 5-minute data block, MF_D is a direction multiplying factor dependent on the opening angle, and TTI is the transverse turbulence intensity for a 3-minute of 5-minute period. Theoretically, the lack of turbulence means a constant direction, thus the "+1" term in Eq 3 is not needed for the angle calculation.

The procedure for the MF_D value selection is analogous to the presented in Section 2.3.4 for the velocity magnitude, starting with the evaluation of a normal distribution, and looking for alternative empirical values if the measured data is not well adapted to the theoretical normal distribution.

3 Results

3.1 Measured fluctuations

Strong fluctuations in the three components of velocity, especially in P2, can be observed in Fig 3, which shows a time history representation of streamwise, transverse and vertical signals for a 3-minute period in P1 and P2 and a 5-minute period in P3 and P4. In the four cases, the figures correspond to a 3-minute or 5-minute averaged velocity magnitude of 1 m/s during flood tide at a distance of 3 m from the sea bottom.

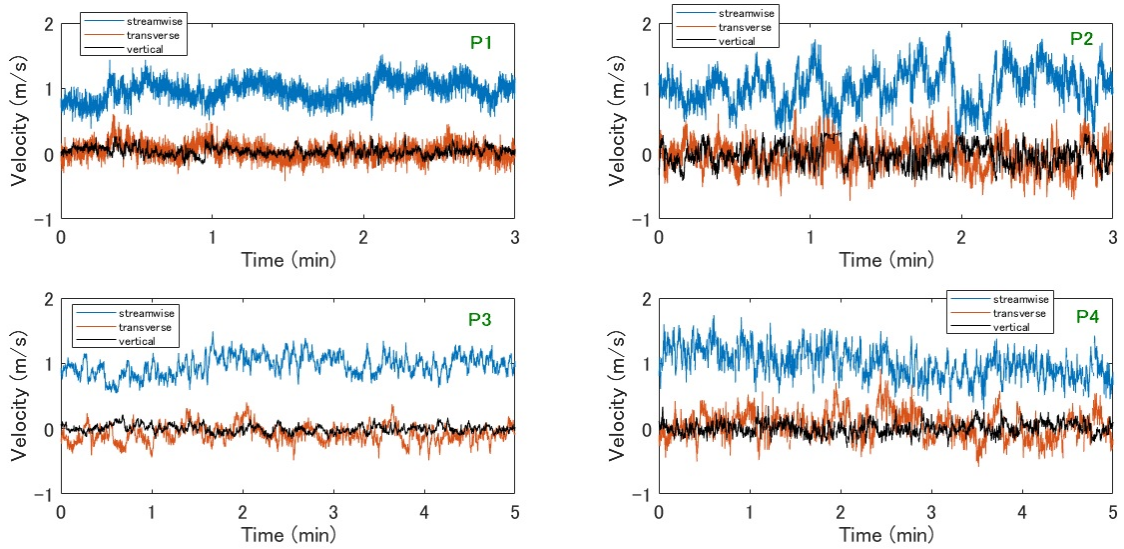

Figure 3: Time fluctuation of streamwise (blue), transverse (red), and vertical (black) for 3 min (P1 and P2) and 5 min (P3 and P4) for which mean velocity magnitude is 1 m/s during flood tide

Table 1 presents velocity magnitude ranges and direction fluctuation angle for the 3-minute and 5-minute periods presented in Fig 3 as well as for other representative depths in the case of P3 and P4, including also ebb tide conditions. In order to avoid the effect of outliers, values shown in Table 1 refer to the gap between percentiles 99.9 and 0.1 for velocity magnitude and the opening angle between percentiles 99.9 and 0.1 for the current direction fluctuation.

In terms of depth dependence, results show a clear tendency, with higher values for range and angle near the seabed due to the bottom effect. This is confirmed with the vertical profiles for velocity magnitude and direction in Fig 4 (P3) and Fig 5 (P4). In this figures, 180° are subtracted to the current directions during ebb tide for an easier comparison with flood results. Magnitude and direction fluctuation gradually increase from the surface to the bottom in flood tide in P4 and in both tide directions in P3. For ebb tide in P4, fluctuation is almost constant throughout the water column, except for depths under 4 m. Also, in P3, for distances from the bottom higher than 20 m, a slightly increase appears due to the effect of water surface.

Comparing conditions at different locations at 3 m from the seabed, magnitude ranges and opening angles are comparable at the four measuring points during ebb tide, while during flood tide clearly higher values are found at P2 and P4 due to the geomorphologic characteristics of the areas surrounding the devices installation spot. More specifically, the presence of a small underwater hill some meters north to P2 in Naru Strait and the convergence of port and channel flows near P4 in Kobe Strait. This characteristic is also clear in the time history plots in Fig 3.

Table 1: Averaged velocity, velocity magnitude range and direction opening angle for flood and ebb tide in P1, P2 and representative depths of P3 and P4

Point	Distance from bottom (m)	Tide direction	Avg velocity (m/s)	Range (m/s)	Direction fluctuation (rad)
P1	3	Flood	0.984	0.885	0.901
		Ebb	1.020	0.913	0.865
P2	3	Flood	1.059	1.594	1.776
		Ebb	1.012	0.778	0.891
P3	3	Flood	0.986	0.822	0.841
		Ebb	0.987	0.998	0.884
	10	Flood	1.243	0.865	0.663
		Ebb	1.231	0.553	0.467
	15	Flood	1.307	0.667	0.369
		Ebb	1.298	0.484	0.411
	20	Flood	1.360	0.580	0.376
		Ebb	1.347	0.620	0.378
P4	3	Flood	1.029	1.284	1.250
		Ebb	1.002	1.093	0.997
	10	Flood	1.480	1.048	0.665
		Ebb	1.126	0.937	0.967
	15	Flood	1.519	0.887	0.575
		Ebb	1.131	0.970	0.862

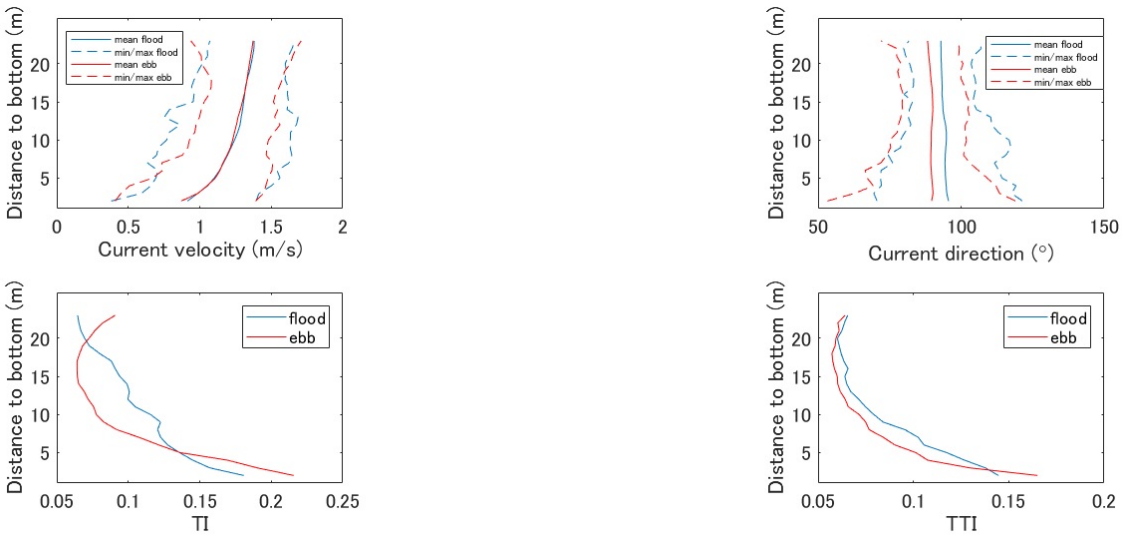

Figure 4: P3 vertical profiles for maximum, minimum and mean velocity magnitude and current direction; TI and TTI

3.2 Prediction of velocity magnitude fluctuation

Time history of turbulence intensity for a tidal cycle at the four measuring points is presented in Fig 6. Excluding slack conditions, turbulence intensity values between 5% and 40% are observed. Regarding data measured at 3 meter from the bottom, a strong variation between ebb and flood conditions is found in P2. To a lesser extent, this effect can be also observed in P3 and P4, where turbulence intensity is slightly higher during

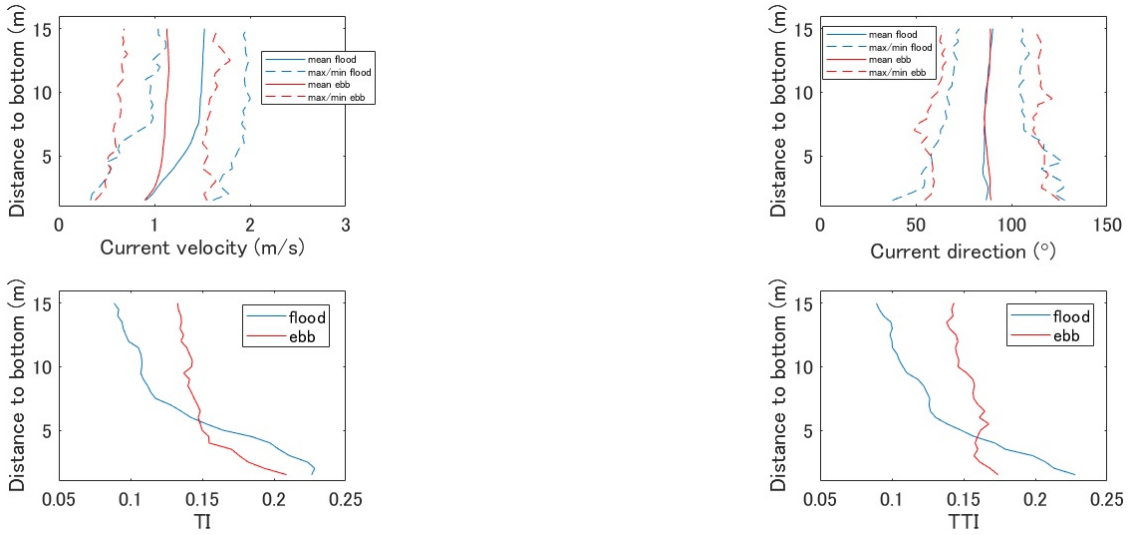

Figure 5: P4 vertical profiles for maximum, minimum and mean velocity magnitude and current direction; TI and TTI

ebb and flood tide, respectively. As stated in Section 3.1, these variations are due to the geomorphological conditions of the area surrounding the measuring point, and have been observed in similar studies for points near the coast [25].

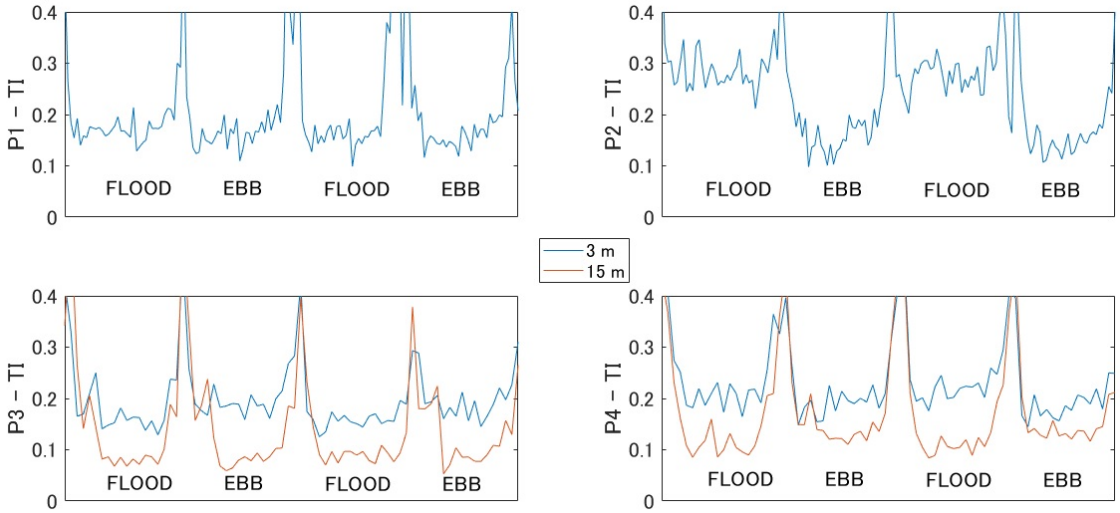

Figure 6: Turbulence intensity time history for a tidal cycle in P1 (3m), P2 (3m), P3 (3m, 15m) and P4 (3m, 15m)

With regard to the dependence on turbulence conditions with depth (P3 and P4), lower turbulence intensity was found at shallower layers. This effect is clearly notable in

Fig 6 for P3, where TI-time representations at 3 m and 15 m follow parallel trends with averaged turbulence intensity values of approximately 15% and 8%, respectively. Similar characteristics are found in P4 during flood tide. However, during ebb tide, due to the confluence of port and channel flows near the measuring point, the influence of horizontal turbulence generator forces is stronger and the gap between shallower and deeper layers due to the bottom effect is lower. The differences between the flows at both depths is also clear in the vertical profiles in 4 and 5. Turbulence intensity decreases from the bottom to shallower depths in P3 and with flood tides in P4 (with the exception of the uppest layers in P3 due to surface effect), while for ebb tide in P4 turbulence intensity decreases from the bottom to nearly 4 m and remains almost constant for shallower layers.

As expected, comparing results for turbulence intensity and velocity magnitude fluctuations (Section 3.2), a clear relation appears. As presented in Section 2.3.4, once this correlation is confirmed, the following analysis aims at finding the value for MF_M in Eq 3 for the various percentiles. The first option is assuming a normal distribution. Skewness and kurtosis analysis are carried out to validate this assumption.

Skewness is parameterized by the Groeneveld and Meeden [28] factor (Eq 6):

$$S_{GM} = \frac{\int_0^{\frac{1}{2}} \left(Q_{1-\alpha} - 2M + Q_\alpha\right) \partial\alpha}{\int_0^{\frac{1}{2}} \left(Q_{1-\alpha} - Q_\alpha\right) \partial\alpha} \tag{6}$$

Where Q is the quantile and M is the median. The percentiles used for this integration are those corresponding with sigma integer multiplying factors for a theoretical normal distribution (0.1, 2.3, 15.9, 84.1, 97.7, 99.9), as well as all the multiple of five from 5 to 95. S_{GM} is bounded by 1 on its absolute values, being zero the value for completely symmetrical data. Results for this skewness factor are represented in Fig 7. Red lines mark the median value, blue boxes limit the area between percentile 25 and percentile 75, and the dot lines show the range from the minimum to the maximum value excluding outliers. Considering the median value of the whole measuring period, skewness factors between -0.05 and 0.05 are found in all the layers and points, without a uniform tendency (slightly positive skew in the lower layers in P4 and deepest layer in P3, slightly negative skew in P1, P2 and all the other layers in P3, and negligible skew from layer 7 to 29 in P4).

Kurtosis is calculated by Eq 7. With this definition, normal distribution data is identified by k=3. Kurtosis lower than 3 means a more outlier-resistant distribution, while for more outlier-prone distributions kurtosis is higher than 3.

$$k = \frac{E\left(x - \mu\right)^4}{\sigma^4} \tag{7}$$

where μ is the mean of x, σ is the standard deviation of x, and E(t) represents the expected value of the quantity t. Following the same procedure as for the skewness factors, median values very close to 3 were found. Only for P1, P2 and the deeper layers in P3 lower k was observed (see Fig 8). This can be attributed to 5-minutes or 3-minutes

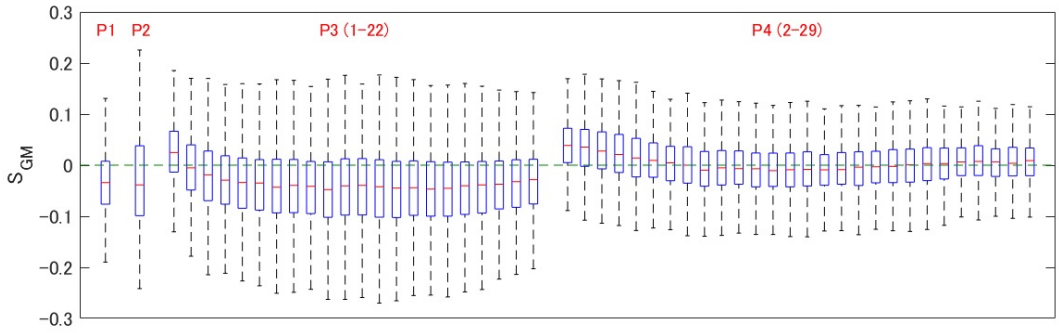

Figure 7: Groeneveld and Meeden skewness factor box plot for velocity magnitude short samples measured in P1, P2, P3 and P4

periods with low averaged velocities ($\bar{V}$ <1 m/s), when the normal distribution bell is cut in its left corner (from zero) due to the lack of negative values. Thus, a good fit of measred data to the normal distribution can be concluded and the corresponding theoretical σ multiplying factor (MF_M) for a given magnitude percentile in a normal distribution can be assumed for its prediction with Eq 4.

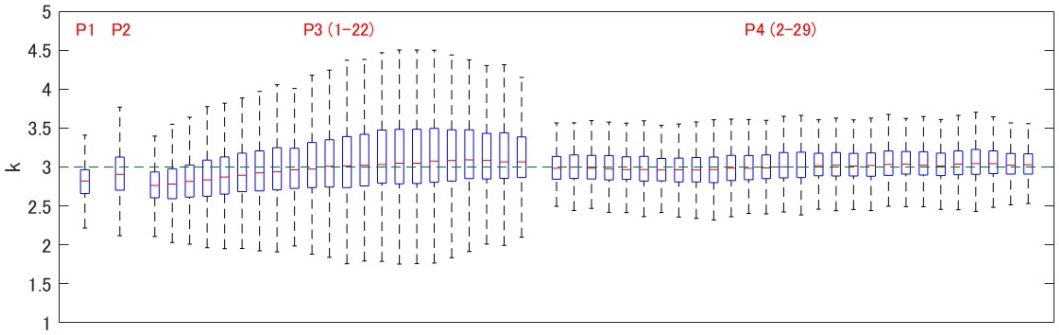

Figure 8: Kurtosis factor box plot for velocity magnitude short samples measured in P1, P2, P3 and P4

The validity of this equation was evaluated by comparing the different percentiles extracted from every 3-minute or 5-minute period with their estimated values. As for skewness and kurtosis analysis, the 52 spatial cases were treated separately (P1, P2, 22 layers in P3 and 28 layers in P4), calculating for each of these cases the prediction levels for 0.1 m/s, 0.15 m/s and 0.25 m/s absolute errors.

The median of the 52 spatial cases prediction levels are presented in Fig 9 for seven representative percentiles. According to these results, velocity magnitude fluctuation fits well with a normal distribution, with prediction levels very close to 100% for the central percentiles of the bell (from 2.3 to 97.7). For percentiles 0.1 and 99.9, a slight variation is observed. An analysis of the errors observed for these two cases is presented in Fig 10. With a median of absolute error close to zero for all the spatial cases, an overestimation

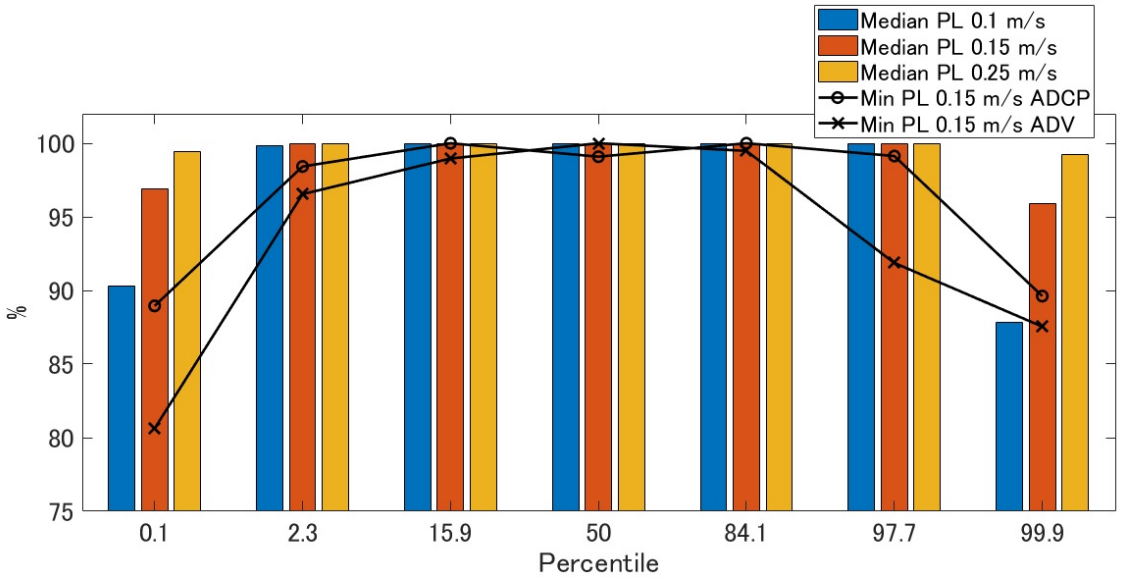

Figure 9: Median value of the 52 prediction levels (Median PL) for margins of error of 0.1 m/s, 0.15 m/s and 0.25 m/s considering a normal distribution for velocity magnitude fluctuation and minimum prediction levels (Min PL) for a margin of error of 0.15 m/s using ADCP and ADV

or underestimation of percentile 99.9 and percentile 0.1 (and by extension to the other percentiles) assuming a normal distribution can be discarded.

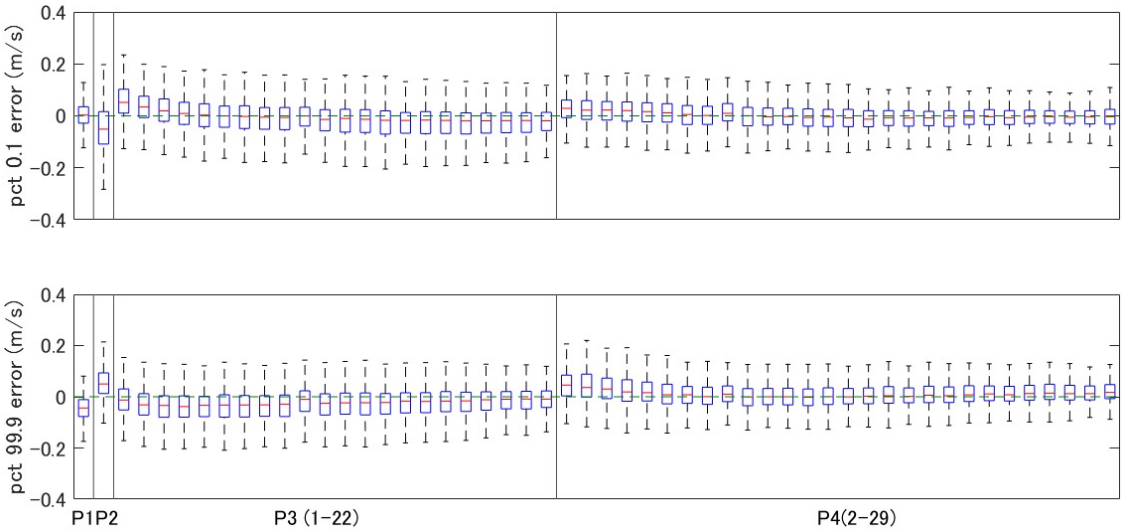

Figure 10: Absolute errors box plot for percentiles 99.9 (pct 99.9) and 0.1 (pct 0.1) of velocity magnitude with the normal distribution assumption

3.3 Prediction of current direction fluctuation

Time history for the same period as for turbulence intensity in Fig 6 is presented in Fig 11 for transverse turbulence intensity. Except for the more pronounced difference between ebb and flood tide conditions in P3 at 3 meter from the bottom or in P4 at both representative depths, results are very similar to those presented in Fig 6. Regarding the vertical profiles, shown in Fig 4 and Fig 5, TTI curves for ebb and flood in P3 are similar, decreasing from the bottom to approximately 12 m from the seabed and remaining almost constant for upper layers. In P4, during flood tide TTI gradually decreases from the bottom to the surface, while for ebb tide it is constant throughout the whole water column. The same characteristics were observed for the variations in current direction for a 3-minute or 5-minute period (Fig 4 and Fig 5), confirming the expected relation between transverse turbulence intensity and current direction fluctuation.

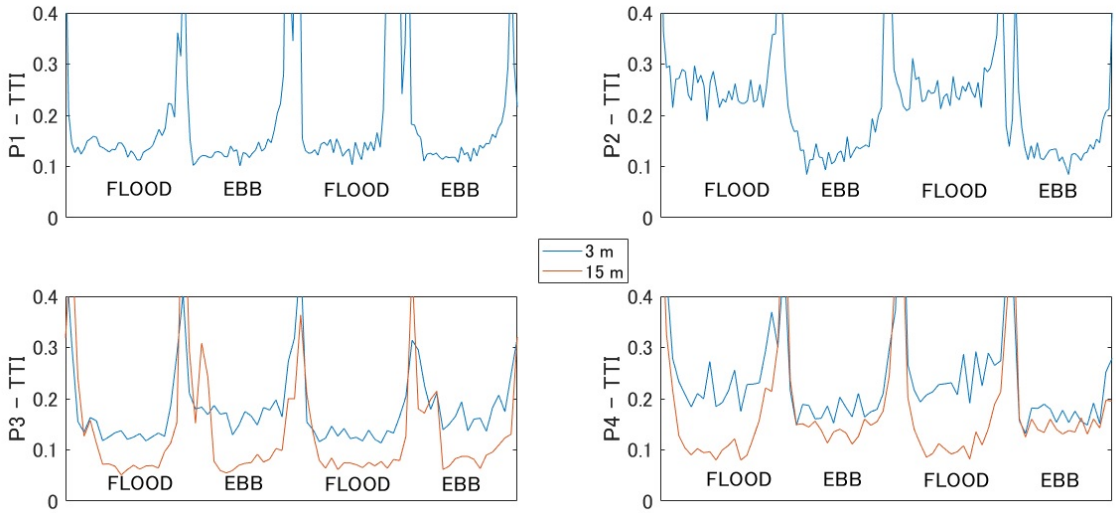

Figure 11: Transverse turbulence intensity time history for a tidal cycle in P1 (3m), P2 (3m), P3 (3m, 15m) and P4 (3m, 15m)

As for velocity magnitude, the adaptability of current direction fluctuation in a short period of time to a normal distribution is evaluated with skewness and kurtosis analysis. Results obtained for skewness evaluation are shown in Fig 12, with coefficients slightly deviatioed from zero for all the cases ($|S|$ <0.05), and without a uniform tendency (positive skew in P4 and the lower layers in P3 and negative skew in the upper layers in P3, P1 and P2). In addition to the evaluation of the adaptability to a normal distribution, this also confirms symmetry in current direction fluctuation for a short period data and validates the assumption established in Section 2.3.3.

Regarding kurtosis, Fig 13 shows values clearly higher than 3 for all the 52 cases, based on which a leptokurtic distribution more outlier-prone than normal can be concluded. Substituting MF_D in Eq 5 by the theoretical σ multiplier factor in a normal distribution for every analyzed opening angle, despite the good adaptability for central

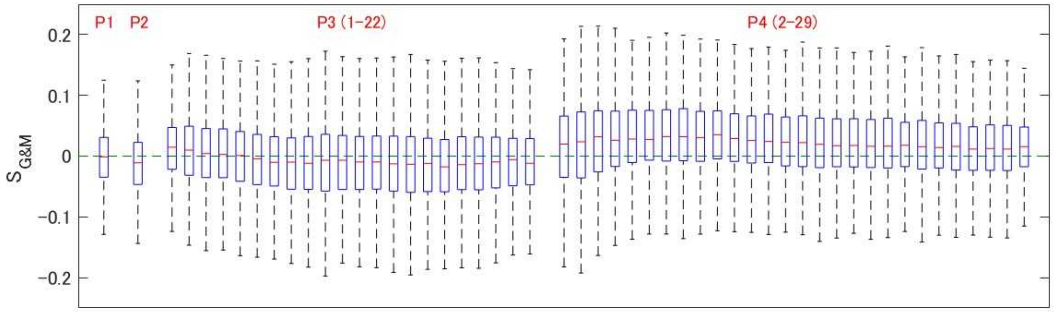

Figure 12: Groeneweld and Meeden skewness factor box plot for velocity direction short samples measured in P1, P2, P3 and P4

angles (55-45 to 90-10), flow direction fluctuation does not fit well with a normal distribution for the widest angles (see Fig 14). Thus, alternative MF_D must be found for the correlation between transverse turbulence intensity and opening angle. The prorated values obtained empirically for each opening angle following the procedure described in Section 2.3.4 and Section 2.3.5 are presented in Table 2.

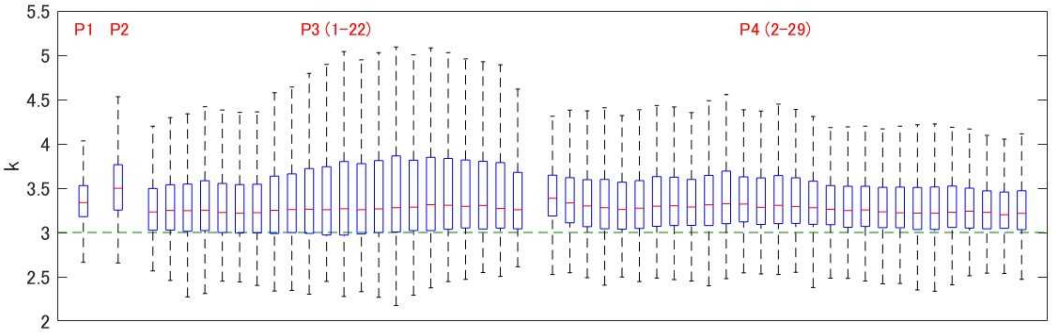

Figure 13: Kurtosis factor box plot for velocity direction short samples measured in P1, P2, P3 and P4

The multiplier factors for the different angles are consistent with the leptokurtic distribution concluded from the kurtosis analysis, with MF_D higher than those in a normal distribution for the three widest angles. This approximation fits more than 75% of 3-minutes or 5-minutes samples with a margin of error of 15% and more than 92% if we consider a margin of 25% from the measured value for the 0.1-99.9 angle. Considering absolute error, results are also clearly better than those observed when compared with the normal distribution, increasing the median of prediction levels for 1°, 2°and 5°in 14, 18 and 21 percentage points. For the 2.3-97.7 angle, the proposed approximation fits more than 77% of samples with a 5% margin of error, increasing to almost 100% for higher margins, as shown in Table 2. For narrower opening angles, with empirical MF_D very close to a normal distribution, error conclusions are similar to those presented in

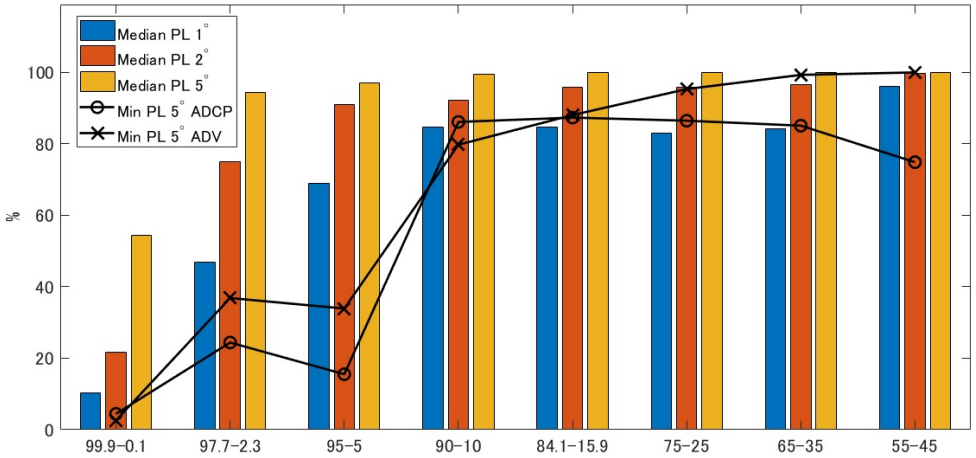

Figure 14: Median value of the 52 prediction levels for margins of error of 1°, 2°and 5°considering a normal distribution for velocity direction fluctuation and minimum prediction levels for a margin of error of 2°using ADCP and ADV

Table 2: Multiplying factor, absolute and relative prediction levels for the different analyzed opening angles

Angle	MF_D (Theo. Normal Distribution)	PL abs 5°(min-max)	PL abs 10°(min-max)	PL rel 15% (min-max)	PL rel 15% (min-max)
99.9-0.1	6.79 (6.00)	0.55-0.89	0.82-0.98	0.75-0.97	0.92-0.99
97.7-2.3	4.17 (4.00)	0.93-1.00	0.98-1.00	0.98-1.00	0.99-1.00
95-5	3.38 (3.29)	0.97-1.00	0.99-1.00	0.99-1.00	0.99-1.00
90-10	2.60 (2.56)	0.99-1.00	0.99-1.00	0.98-1.00	0.99-1.00
85-15	2.08 (2.07)	0.99-1.00	0.99-1.00	0.97-1.00	0.98-1.00
84.1-15.9	2.01 (2.00)	0.99-1.00	0.99-1.00	0.97-1.00	0.98-1.00
80-20	1.68 (1.68)	0.99-1.00	0.99-1.00	0.97-1.00	0.98-1.00
75-25	1.37 (1.35)	0.99-1.00	0.99-1.00	0.97-1.00	0.98-1.00
70-30	1.08 (1.05)	0.99-1.00	0.99-1.00	0.97-1.00	0.98-1.00
65-35	0.81 (0.77)	0.99-1.00	1.00-1.00	0.97-1.00	0.98-1.00
60-40	0.54 (0.51)	0.99-1.00	1.00-1.00	0.97-1.00	0.98-1.00
55-45	0.27 (0.25)	1.00-1.00	1.00-1.00	0.98-1.00	0.99-1.00

Fig 14. Focusing in the widest angle, for which the highest difference with the measured data is found, a deeper error analysis is presented in Fig 15. For all the 52 cases, median values are close to zero, with a highest median relative error of 4.82% in the eighth layer in P3 and a lower of -4.97% in P2. Thus, as for the velocity magnitude fluctuation prediction method, overestimation or underestimation can be discarded.

4 Discussion

The new methods are evaluated by comparing the results from the estimation by Eq 3 and Eq 5 with measured data for velocity magnitude percentiles and opening angles, respectively.

Regarding velocity magnitude fluctuation, Fig 16 shows a comparison of velocity magnitude measured and estimated values for the 0.1 and 99.9 percentiles during the

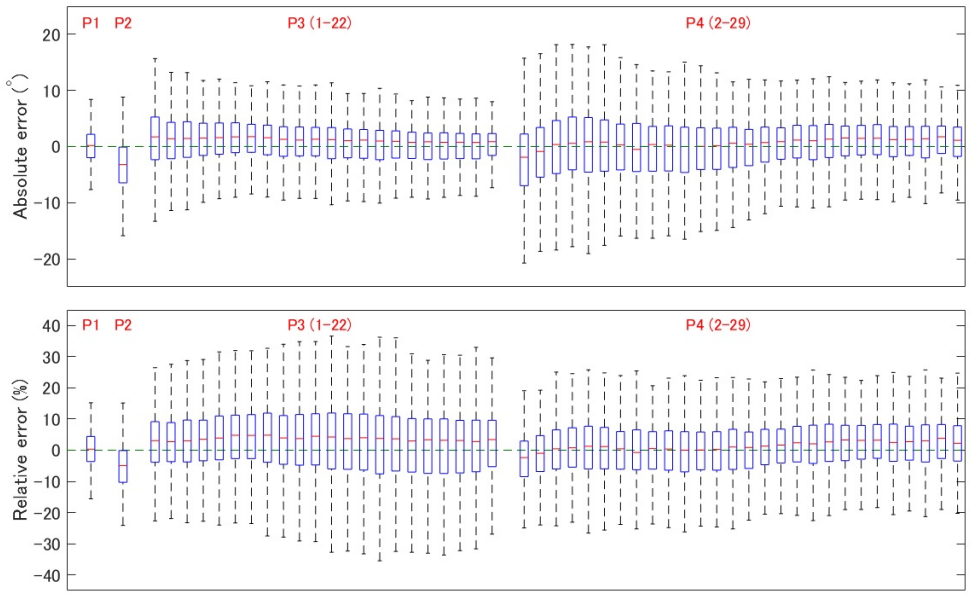

Figure 15: Absolute and relative errors box plot for pct 99.9 - pct 0.1 opening angle estimation with the empirical multiplying factor

measuring period in P2. Even in the worst scenario (percentiles with the lower prediction levels and the measuring point with the highest median error), red line shows a very good agreement with measured data, giving an idea of the high accuracy of this estimation method. In Fig 16, it is also notable the important difference between flood and ebb, with good results for both tide directions, which shows the capability of this method for diverse flow conditions.

Similarly, a comparison of measured and estimated values for the three widest angles in P2 is shown in Fig 17, for which values corresponding with 3-minute averaged velocity lower than 0.7 m/s are discarded. As in Fig 16, the difference between ebb and flood tides is notable, getting a very good correlation for both flow conditions. Since these three opening angles show the lowest prediction levels according to information provided in Table 2, a better agreement is expected for narrower angles and other spatial cases.

For current direction fluctuation prediction by numerical modelling, a turbulence anisotropic ratio (σ_s:σ_t:σ_v) needs to be assumed. As presented in Section 2.3.5, Nezu and Nakagawa [27], based on an experimental study with two-dimensional channel flows at relatively low Reynolds numbers, proposed the ratios 1:0.71:0.55. Regarding data measured in strong tidal channels, Milne et al [8] observed 1:0.75:0.56 ratios for current velocities around 2 m/s. The ratios calculated from the data measured for the present study for the 3-minute data blocks representative of flood conditions at 1 m/s shown in Table 1 are 1:0.85:0.45 for P1 and 1:0.78:0.58 for P2. Concerning the data measured by ADCP, vertical averaged ratios are 1:0.79:0.40 for P3 and 1:0.98:0.41 for P4. Except for P4, both the ratios shown in [8] and measured in the present study agree relatively

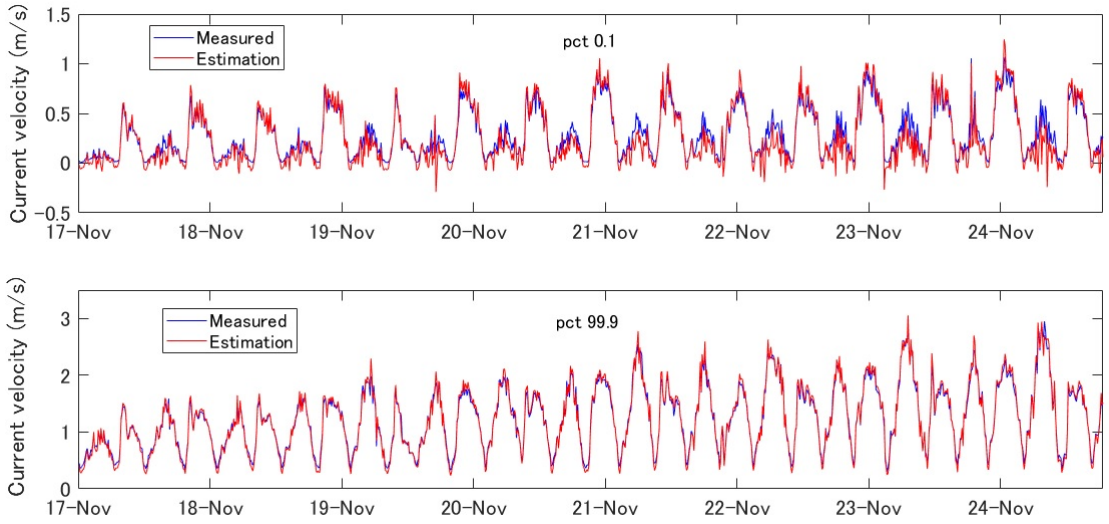

Figure 16: Comparison of measured (blue) data and estimation (red) values for percentiles 99.9 (pct 99.9) and 0.1 (pct 0.1) of velocity magnitude

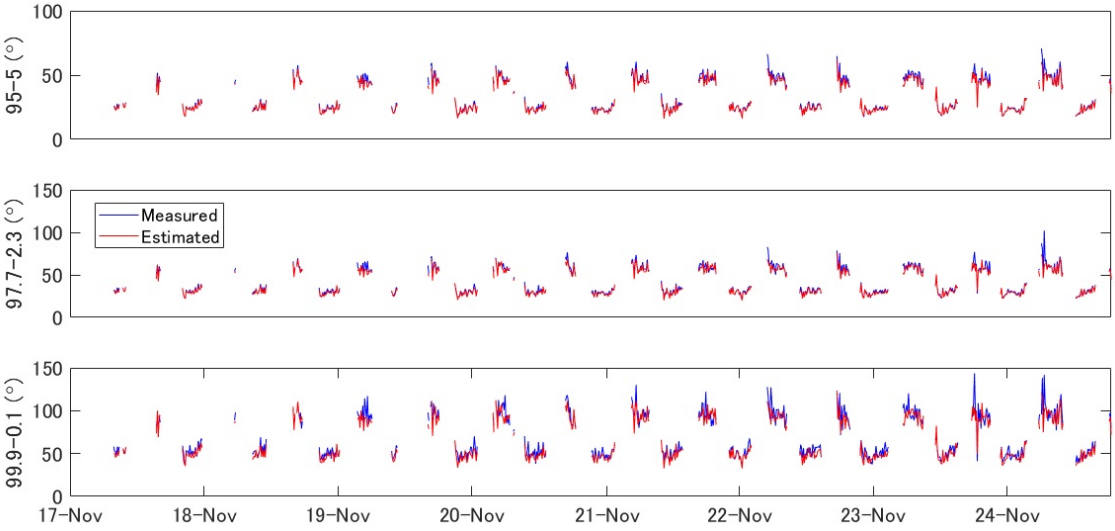

Figure 17: Comparison of measured (blue) data and estimation (red) values for opening angles 99.9-0.1, 97.7-2.3 and 95-5

well with those proposed by Nezu and Nakagawa [27], with the expected deviations from the theoretical ratios due to the differences in bathymetry and Reynolds numbers. In the case of P4, due to the shallower and narrower nature of the channel, the irregular shape of the coastline (multiple small capes and gulfs) and the variable depth (hills and valleys in various directions), the fluctuation in the transverse component of velocity

becomes more important. These differences in the turbulence anisotopic ratios must be considered when applying this method to the prediction of current direction fluctuation by numerical modelling.

5 Conclusions

Within the journey towards tidal energy stream commercial exploitation, one of the main topics is the adaptability of laboratory devices to sea water and flow conditions. In this regard, some converters have had to face issues related to biofouling, marine corrosion or turbulence conditions. Concerning this last topic, notable turbulence-related high frequency fluctuations in velocity magnitude and direction have been observed by in-situ measurements. The present paper analyzes this fluctuation and introduces a new method for its estimation based on short data samples measured by two ADVs and two ADCPs at 4 different locations with diverse flow conditions in the waters of Goto Islands, Japan.

Dividing measured data into 3-minutes (ADV) and 5-minutes (ADCP) samples, magnitude fluctuation is well adapted to a theoretical normal distribution. With this assumption, more than 80% percentiles 0.1 and 99.9 can be predicted within a margin of error of 0.15 m/s. This percentage increases to values very close to 100% for more centered percentiles (2.3, 97.7, 5, 95,...). For direction fluctuation, data samples show a leptokurtic distribution, which implies a greater importance of outliers. Thus, the normal distribution assumption showed good results for central opening angles (from percentiles 45-55 to percentiles 10-90), whilst for wider angles there is an underestimation problem. The three widest angles (5-95, 2.3-97.7, 0.1-99.9) were treated empirically, obtaining slope trends of 3.38, 4.17 and 6.79, respectively, instead of 3.29, 4 and 6 of the theoretical normal distribution. With these new factors, more than 75% of the 99.9-0.1 and more than 98% of 97.7-2.3 opening angles can be estimated with a 15% margin of error. These results demonstrate the validity of this method for the estimation of this kind of fluctuation, regardless of measuring device, frequency sampling, location or depth.

The importance of this work lies not only in the understanding of this kind of fluctuations, but also in the relation of these with turbulence intensity for magnitude and transverse turbulence intensity for direction. Since both parameters can be calculated indirectly by numerical models, the conclusions extracted from this paper represent a significant step towards tidal stream energy commercialization. Reducing the need for in-situ measurements, this new prediction method allows a higher accuracy in energy resource prediction (residuals from harmonic analysis up to 5 kW/m^2 have been observed in a tidal site with maximum velocity of 3 m/s [10]) and an important advance concerning converters design, since high frequency fluctuations in velocity have an important effect on the device stabilization [12] and on the dynamic loading conditions on the blades, support structures and seabed connections [11].

Acknowledgements

The authors would like to thank the Ministry of Environment of Japan for permission to publish of the data used in this study, which were obtained through the project for Promotion of Realization of Tidal Current Power Generation supported by the ministry in 2014 and 2015.

References

[1] Foreman M.G.G, *Manual for tidal heights analysis and prediction*. Technical Report Pacific Marine Science Report 77-10, Institute of Ocean Sciences, Patricia Bay, Sidney B.C..

[2] Pawlowicz R., Beardsley B., Lentz S., *Classical tidal harmonic analysis including error estimates in MATLAB using T_TIDE*, Computers and Geosciences 28 (2002), 929-937.

[3] Matsumoto K., Takanezawa T., Ooe M., *Ocean tide models developed by assimilating TOPEX/POSEIDON altimeter data into hydrodynamical model: a global model and a regional model around Japan*, J. Oceanography 56 (2000), 567-581.

[4] Coles D.S., Blunden L.S., Bahaj, A.S., *Assessment of the energy extraction potential at tidal sites around the Channel Islands*, Energy 124 (2017) 171-186.

[5] Perez-Ortiz A., Borthwick A.G.L., McNaughton J., Avdis A., *Characterization of the tidal resource in Rathlin Sound*, Renewable Energy 114 (2017) 229-243.

[6] Carballo R., Iglesias G., Castro A., *Numerical model evaluation of tidal stream energy resources in the Ria de Muros (NW Spain)*, Renewable Energy 34-6 (2009) 1517-1524.

[7] Godin G., *On the predictability of currents*, International Hydrographic Review 60 (1983) 119-126.

[8] Milne I.A., Day A.H., Sharma R.N, Flay R.G.J., *Blade loading on tidal turbines for uniform unsteady flow*, Renewable Energy 77 (2015) 338-350.

[9] CBC News, *Failed tidal turbine explained at symposium*, https://www.cbc.ca/news/canada/nova-scotia/failed-tidal-turbine-explained-at-symposium-1.1075510, 2011 (accessed 1 Sept 2018)

[10] Polagye B., Epler J., Thomson J., *Limits to the predictability of tidal current energy*, In OCEANS 2010 (2010) 1-9.

[11] Harding S., Thomson J., Polagye B., Richmond M., Durgesh V., Bryden I., *Extreme value analysis of tidal stream velocity perturbations*, In Proceedings of the 9th EWTEC (2011).

[12] Owen A., Bryden I., *Prototype support structure for seabed mounted tidal current turbines*, Proceedings of the Institution of Mechanical Engineers Part M: Journal of Engineering for the Maritime Environment 219-4 (2005) 173-183.

[13] Mycek P., Gaurier B., Germain G., Pinon G., Rivoalen E., *Experimental study of the turbulence intensity effects on marine current turbines behaviour. Part I: one single turbine*, Renewable Energy 66 (2014) 729-746.

[14] Blackmore T., Batten W.M.J., Bahaj A.S., *Influence of Turbulence on the Wake of a Marine Current Turbine Simulator*, Proceedings. Mathematical, Physical, and Engineering Sciences / The Royal Society 470.2170 (2014): 20140331. doi:10.1098/rspa.2014.0331.

[15] Blackmore T., Myers L.E., Bahaj A.S., *Effects of turbulence on tidal turbines: Implications to performance, blade loads, and condition monitoring*, International Journal of Marine Energy 14 (2016) 1-26.

[16] Pyakurel P., VanZwieten J.H., Dhanak M., Xiros N.I., *Numerical modeling of turbulence and its effect on ocean current turbines*, International Journal of Marine Energy 17 (2017) 84-97.

[17] Milne I.A., Sharma R.N., Flay R.G.J., Bickerton S., *Characteristics of the turbulence in the flow at a tidal stream power site*, Philos. Trans. R. Soc. A 371 (2013) 1-14.

[18] Garcia-Novo P., Kyozuka Y., *Field measurement and numerical study of tidal current turbulence intensity in the Kobe Strait in Goto Islands, Nagasaki Prefecture*, J Mar Sci Technol 22 (2017) 335 -350, DOI 10.1007/s00773-016-0414-x.

[19] Togneri M., Lewis M., Neill S.P., Masters I., *Comparison of ADCP observations and 3D model simulations of turbulence at a tidal energy site*, Renewable Energy 114A (2017) 273-282.

[20] Waldman S., Yamaguchi S., O'Hara Murray R., Woolf D., *Tidal resource and interactions between multiple channels in the Goto Islands, Japan*, International Journal of Marine Energy 19 (2017) 332-344.

[21] Garcia-Novo P., Kyozuka Y., *Analysis of turbulence and extreme current velocity values in a tidal channel*, Journal of Marine Science and Technology (2018). https://doi.org/10.1007/s00773-018-0601-z.

[22] Rusello P.J., *A practical primer for pulse coherent instruments*, Nortek technical note TN-027. NortekUSA (2009), USA.

[23] *Nortek Signature 1000/500/250 Operations Manual*, www.nortek-as.com/lib/manuals/signature1000-500-operations-manual, 2017 (accessed 1 Sept 2018).

[24] Islam, Zhu, *A Kernel Density Based Algorithm to Despike ADV Data*, J. of Hydraulic Eng 139-7 (2014) 785-798.

[25] Thomson J., Polagye B., Durgesh V., Bickerton M.C., *Measurements of turbulence at two tidal energy sites in Puget Sound, WA*, IEEE J. Oceanic Eng 37-3 (2012) 363-374.

[26] Ramos V., Carballo R., Alvarez M., Sanchez M., Iglesias G., *A port towards energy self-sufficiency using tidal stream power*, Energy 71 (2014) 432-444.

[27] Nezu I., Nakagawa H., 1993. *Turbulence in open-channel flows*, A. A. Balkema, Rotterdam, The Netherlands.

[28] Groeneveld R.A., Meeden G., *Measuring skewness and kurtosis*, Statistician 33 (1984) 391–399.